

# Electron-Cyclotron-Maser Observable Modes

A. Stupp

*School of Physics and Astronomy, Tel-Aviv University, Israel*

11 September 2021

## ABSTRACT

We investigated wave amplification through the Electron-Cyclotron-Maser mechanism.

We calculated absorption and emission coefficients without any approximations, also taking into account absorption by the ambient thermal plasma. A power-law energy distribution for the fast electrons was used, as is indicated by X-ray and microwave observations.

We developed a model for the saturation length and amplification ratio of the maser, scanned a large parameter space, and calculated the absorption and emission coefficients for every frequency and angle.

Previous studies concluded that the unobservable Z-mode dominates in the  $\nu_p \approx \nu_B$  region, and that millisecond spikes are produced in the region  $\nu_p/\nu_B < 0.25$ . We find that the observable O-mode and X-mode can produce emission in the  $0.8 < \nu_p/\nu_B < 2$  region, which is expected at the footpoints of a flaring magnetic loop.

The important criterion for observability is the saturation length and not the growth rate, as was assumed previously, and even when the Z-mode is the most strongly amplified, less strongly amplified O-mode or X-mode are still intense enough to be observed.

The brightness temperature computed with our model for the saturation length is found to be of order  $10^{16}$  K and higher. The emission is usually at a frequency of  $2.06\nu_B$ , and at angles 30–60 degrees to the magnetic field. The rise time of the amplified emission to maximum is a few tenths of a millisecond to a few milliseconds, and the emission persists for as long as new fast electrons arrive into the maser region.

**Key words:** Sun : flares – Sun : radio radiation – masers – radiation mechanisms : non-thermal – instabilities – methods : numerical

## 1 INTRODUCTION

Electromagnetic emission generated by relativistic electrons moving in a magnetic field is referred to as *synchrotron* radiation if the electrons are ultra-relativistic, and as *gyrosynchrotron* if the electrons are mildly relativistic. In the present paper we deal only with gyrosynchrotron radiation, using the formalism developed by Ramaty ( 1969), except that we also include the longitudinal component of the radiation which is important at low multiples of the cyclotron frequency. We also take into account the correction pointed out by Trulsen and Fejer ( 1970). This formalism has been tested by other workers (e.g. Holman & Benka 1992) and was found to be accurate. Gyrosynchrotron absorption can become negative and this amplification process is referred to as the Electron-Cyclotron-Maser (ECM).

The observation of millisecond microwave spikes from the Sun (reviewed by Benz 1986) has been interpreted as gyrosynchrotron maser emission since the late 1970's (Wu & Lee 1979; Holman, Eichler & Kundu 1980), and it is now the most widely accepted explanation for the spike emission

(Benz 1993). Spikes have been observed in the frequency range 0.3–8 GHz, exhibit a duration of a few milliseconds to a hundred milliseconds, a narrow bandwidth (0.5–2 per cent or a few MHz), and until recently have not been resolved in angle (Benz et.al. 1996). By assuming that the homogeneity scale of the magnetic field is of order  $10^7$  cm, and that this is the size of the source, it is possible to deduce a characteristic brightness temperature of  $10^{15-18}$  K .

In order that ECM appears the electron number distribution must either increase towards higher energies or an anisotropy in pitch angle must exist, as in a loss cone distribution. A loss cone forms naturally where the magnetic field increases, as electrons with small pitch angles continue and electrons with large pitch angles mirror. At the footpoints of flare loops the density becomes high enough that electrons continuing into the chromosphere lose their energy and do not reflect back upwards, and thus a loss-cone distribution appears (Aschwanden & Benz 1988; Kuncic & Robinson 1993). We therefore expect maser emission from the region of the footpoints.

The study of the ECM mechanism is of interest because

of the radio emission, which serves as a probe into conditions in the flare, and also because of the energetic particle precipitation which produces X-rays, and for local heating of coronal material. The ECM reduces the trapping time and increases the flux of precipitating particles by causing a reduction in the pitch angle of electrons within a short distance (Benz 1993). Electrons which otherwise would be mirrored back and forth are thus precipitated into the chromosphere after one reflection. The maser thus transfers energy from the fast particle distribution to the ambient plasma, and serves as a heating mechanism.

Several papers have explored the possibilities of ECM. Melrose and Dulk (1982) have used a semi-relativistic approximation to derive approximate formulae for the frequency of the largest growth rate, and for the growth rate. Winglee (1985) approximated the effects of the ambient plasma temperature on the maser emission. Aschwanden (Aschwanden 1990a,b) followed the diffusion of electrons into the loss-cone as a result of the maser emission, and therefore the self-consistent closure of the loss-cone as kinetic energy is transformed to radiation through the maser. Aschwanden (1990b) concluded that the millisecond spikes are produced in the region of  $\nu_p/\nu_B < 0.25$ . Kuncic and Robinson (1993) performed ray-tracing in a model loop with dipole field, and concluded that maser emission can escape from lower levels. Fleishman and Yastrebov (1994a) present results which show simultaneous amplification in two or more frequencies.

An important difference in our work is that all previous studies concentrated on the *growth rate* of the amplified wave, and defined the *dominant mode* as the particular wave – frequency  $\nu$  and direction to the magnetic field  $\theta$  – with the largest growth rate. However, the important criterion for long-term emission is the *saturation length*, which is the distance beyond which the maser ceases to amplify, and not the growth rate (Benz 1993). We compute the absorption coefficient and, using our model, the saturation length, and determine which wave will be observed, and at what intensity.

Another difference is that most previous studies used soft energy distributions for the fast electrons, such as the Dory, Guest, Harris distribution (Winglee & Dulk 1986) or a hot thermal component distribution (Aschwanden 1990a,b). However, observations of Microwaves (MW) and X-rays from solar flares indicate a power law energy spectrum with energy up to 10 MeV and even higher, and with a power index typically  $\delta = 3$ , and in the range  $\delta = 2 - 6$  (Ramaty 1969; Zirin 1989; Fleishman & Yastrebov 1994b for other references). We therefore chose to use a power law distribution function for our fast non-thermal electrons. We also use an idealized one sided loss-cone distribution (Melrose & Dulk 1982) while other studies use a one sided  $\sin^N(\phi)$  distribution (Aschwanden 1990a,b) or a two-sided gaussian (Fleishman & Yastrebov 1994a,b) pitch angle distribution.

The ratio  $\nu_p/\nu_B$ , where  $\nu_p = \sqrt{n_e/m/\pi} e$  is the plasma frequency and  $\nu_B = eB/(m\gamma c)/(2\pi)$  the cyclotron frequency, is an important parameter for ECM emission. It is used to distinguish regions where different magneto-ionic modes dominate. From the previous studies we conclude that the dominant mode depends on the distribution function of the fast electrons. In some studies the fundamental eXtraOrdinary (XO) mode is dominant for  $\nu_p/\nu_B < 0.3$

(Aschwanden & Benz 1988), while in others the fundamental Ordinary Mode (OM) is dominant for  $\nu_p/\nu_B < 0.5$  (Winglee & Dulk 1986). In some the fundamental OM is dominant for  $0.3 < \nu_p/\nu_B < 1$  (Aschwanden & Benz 1988), and in others the second harmonic XO is dominant for  $0.5 < \nu_p/\nu_B < 1.5$  (Winglee & Dulk 1986). The unobservable Z-Mode (ZM) is dominant for  $\nu_p/\nu_B > 1.5$  (Winglee & Dulk 1986), or even for  $\nu_p/\nu_B > 0.5$  (Fleishman & Yastrebov 1994b). In our work the ZM is the most highly amplified mode (i.e. with the largest in absolute value negative absorption) for the range  $0.5 < \nu_p/\nu_B < 1.1$  and for  $1.8 < \nu_p/\nu_B$ , similar to what was found by others who have used a power law (Fleishman & Yastrebov 1994b).

The high amplification of the ZM would seem to indicate that this unobservable mode is the dominant mode, and would therefore preclude the maser mechanism as the producer of MW spikes, except in the narrow range  $1.1 < \nu_p/\nu_B < 1.8$ . We show that for the range  $\nu_p/\nu_B < 2$  it is possible for the OM or the XO mode to be amplified enough that they become observable. Our absorption-coefficient approach allows a simple procedure to estimate the saturation length, which is difficult to derive from growth rate calculations, and is the important parameter in deciding which mode dominates (Benz 1993). Our derived saturation lengths are consistent with the assumed homogeneity of the magnetic field and density. We therefore conclude that the Electron-Cyclotron-Maser mechanism can produce microwave spikes.

In section 2 we give the theory and equations for gyrosynchrotron emission and wave propagation through cold-plasma. In section 3 we show that the gyrosynchrotron is the important process in absorption as well as emission, for the frequencies and plasma parameters we assume. Section 4 describes our estimate of the energy available to the loss-cone, and a derivation of the saturation length is given. Section 5 describes our calculations and the parameters we used. In section 6 we discuss the observability of the maser emission under different conditions, in section 7 we give a comparison with previous studies, and in section 8 we summarize our results.

## 2 GYROSYNCHROTRON ABSORPTION

Solar flares are known to be a complex phenomena. The solar flare plasma is composed of both an ambient thermal plasma, and a population of fast particles. It is customary to simplify and assume that any waves which are excited are a phenomena of the ambient plasma alone. The properties of the ambient plasma therefore determine which waves are excited and how the waves propagate. However, the fast particles can absorb waves present in the ambient plasma, and also emit in these waves' frequencies. We used the cold plasma approximation to describe the ambient plasma, and assumed the waves which result from magnetoionic theory (Melrose 1989). For a given electron distribution  $f(\mathbf{p})$  and wave  $(\nu, \theta)$  it is then possible to compute the emission and absorption coefficients, which describe the interaction of the wave with the distribution.

The cold plasma parameters which determine the propagation are the refraction index and the components of the

polarization vector (Melrose 1989):

$$\hat{\epsilon}_\sigma = \frac{L_\sigma(\mathbf{k})\hat{k} + T_\sigma(\mathbf{k})\mathbf{t} + i\mathbf{c}}{\sqrt{1 + L_\sigma^2 + T_\sigma^2}} \quad (1)$$

where  $\mathbf{k}$  is the wave vector,  $\hat{k}$  a unit vector in the  $\mathbf{k}$  direciton,  $\mathbf{c}$  a unit vector perpendicular to  $\mathbf{k}$  and to the magnetic field  $\mathbf{B}$ , and  $\mathbf{t}$  is a unit vector perpendicular to  $\mathbf{k}$ , in the plane of  $\mathbf{k}$  and  $\mathbf{B}$ . Also  $T_\sigma$  and  $L_\sigma$  are functions depending on  $\mathbf{k}$ , and  $\sigma$  is '+' (OM) or '-' (XO mode). The transverse component of the polarization is given by  $T_\sigma$  and the longitudinal component is described by  $L_\sigma$ . We assumed  $\mathbf{B}$  to be in the  $\hat{z}$  direction, and  $\mathbf{k}$  to be in the  $(x, z)$  plane with angle  $\theta$  to the magnetic field. With these definitions  $\mathbf{c} = \hat{y}$ ,  $\hat{k} = (\sin(\theta), 0, \cos(\theta))$ , and  $\mathbf{t} = (\cos(\theta), 0, -\sin(\theta))$ .

The cold plasma modes are the OM, which exists for

$$\nu > \nu_p \quad (2)$$

the XO which exists for

$$\nu > \nu_x = \nu_B/2 + \sqrt{\nu_p^2 + \nu_B^2/4} \quad (3)$$

and the low frequency branch of the XO, called here the ZM, which exists for

$$\nu_x - \nu_B < \nu < \sqrt{0.5} \times \sqrt{(\nu_p^2 + \nu_B^2) + [(\nu_p^2 + \nu_B^2)^2 - 4\nu_p^2\nu_B^2 \cos^2(\theta)]^{0.5}}$$

and is bound from above by the upper-hybrid frequency

$$\nu_{uh} = \sqrt{\nu_B^2 + \nu_p^2} \quad (4)$$

The Whistler mode exists for

$$\nu < \sqrt{\frac{(\nu_p^2 + \nu_B^2) - [(\nu_p^2 + \nu_B^2)^2 - 4\nu_p^2\nu_B^2 \cos^2(\theta)]^{0.5}}{2}} \quad (5)$$

and is a low frequency mode which we ignore (Melrose 1989).

The equations for the cold-plasma parameters are (Ramaty 1969; Melrose 1989)

$$T_\pm = [2\nu(\nu_p^2 - \nu^2) \cos(\theta)] \times \left[ -\nu^2 \nu_B \sin^2(\theta) \pm \sqrt{\nu^4 \nu_B^2 \sin^4(\theta) + 4\nu^2(\nu_p^2 - \nu^2)^2 \cos^2(\theta)} \right]^{-1} \quad (6)$$

$$L_\pm = \frac{\nu_p^2 \nu_B \sin(\theta)}{\nu^3 - \nu \nu_p^2} \frac{\nu T_\pm}{\nu T_\pm - \nu_B \cos(\theta)} \quad (7)$$

And the refraction index  $n_{ref}$ , also referred to as  $n_\pm$ , is given by

$$n_\pm^2 = 1 + [2\nu_p^2(\nu_p^2 - \nu^2)] \times \left[ -2\nu^2(\nu_p^2 - \nu^2) - \nu^2 \nu_B^2 \sin^2(\theta) \pm \sqrt{\nu^4 \nu_B^4 \sin^4(\theta) + 4\nu^2 \nu_B^2(\nu_p^2 - \nu^2)^2 \cos^2(\theta)} \right]^{-1} \quad (8)$$

With the symbols being  $\nu_p$  the plasma frequency,  $\nu_B$  the cyclotron frequency, and  $\nu$  the emitted frequency.

The cold plasma approximation is valid only if the two following criteria are true (Melrose 1989)

$$\left( \frac{\nu - s\nu_B}{n_{ref}\nu \cos(\theta)} \right)^2 >> \frac{k_B T}{m_e c^2} = 0.001683 \frac{T}{10^7 \text{ K}} \quad (9)$$

and

$$\left( \frac{\nu_B}{n_{ref}\nu \sin(\theta)} \right)^2 >> \frac{k_B T}{m_e c^2} = 0.001683 \frac{T}{10^7 \text{ K}} \quad (10)$$

Where we have used  $k_{||} = n_{ref}\omega \cos(\theta)/c$  and  $v_{thermal} = \sqrt{k_B T/m_e}$  to get the above from Melrose's equations. The  $s$  multiplier in the first criterion is an integer such that  $s\nu_B$  is the closest cyclotron harmonic to  $\nu$ .

Our rule for when the cold plasma approximation ceases to be valid is when the left side of the criteria is less then ten times larger than the right side. The cold plasma approximation fails near the resonances of the cold plasma modes at the cyclotron harmonics, and for the low-frequency Z-mode when the frequency of the waves is near the upper-hybrid frequency.

Most authors calculate the growth rate, but our derivation follows Ramaty's (1969) in calculating the absorption coefficient which is (Ramaty 1969; Aschwanden 1990a):

$$k_\pm(\nu, \theta) = \frac{1}{B} 4\pi^2 e \frac{2\pi}{|\cos(\theta)|} \frac{\nu_B}{\nu} \frac{1}{n_\pm^2} \int_1^\infty d\gamma \frac{u(\gamma)}{\beta} \times \sum_{s=s_1}^{s_2} \frac{g(\phi_s)}{1 + T_\pm^2} \left[ \beta \sin(\phi_s) J'_s(x_s) + \frac{L_\pm}{n_\pm} J_s(x_s) + T_\pm \left( \frac{\cot(\theta)}{n_\pm} - \frac{\beta \cos(\phi_s)}{\sin(\theta)} \right) J_s(x_s) \right]^2 \times \left[ \frac{-\beta \gamma^2}{u(\gamma)} \frac{d}{d\gamma} \frac{u(\gamma)}{\beta \gamma^2} + \frac{n_\pm \beta \cos(\theta) - \cos(\phi_s)}{\gamma \beta^2 \sin(\phi_s)} \frac{1}{g(\phi_s)} \frac{dg(\phi)}{d\phi} \right] \quad (11)$$

Where we corrected Ramaty's (1969) formula by deleting a factor  $1 + \partial \ln(n_{ref})/\partial \ln(\nu)$ , and changed the minus sign multiplying the  $J'_s$  term because our  $T_\pm$  have the opposite sign to Ramaty's  $a_{\theta\pm}$ . We also added the longitudinal contribution which is important for frequencies close to the cyclotron frequency.  $J_s$  are Bessel functions,  $J'_s$  their derivatives, with the argument  $x_s = (\nu/\nu_B)n_\pm \gamma \beta \sin(\theta) \sin(\phi_s)$ . The limits of the summation are  $s_1, 2 = \frac{2\nu}{\nu_B} [1 \pm n_{ref} \beta \cos(\theta)]$ , and  $\pm$  designates the mode ('+' for OM and '-' for XO). The angle  $\phi_s$  comes from the resonance condition (Ramaty 1969; Melrose 1989)

$$\frac{s\nu_B}{\gamma} = \nu [1 - n_{ref} \beta \cos(\theta) \cos(\phi)] \quad (12)$$

and is derived by

$$\cos(\phi_s) = \frac{1 - \frac{s\nu_B}{\gamma\nu}}{n_\pm \cos(\theta) \beta} \quad (13)$$

The distribution function of the electrons was assumed to be separable into the form

$$f(\mathbf{p}) d^3 p = 2\pi u(\gamma) g(\phi) d\gamma d(\cos(\phi)) \quad (14)$$

Where  $\phi$ , the pitch angle, is the angle of the velocity to the magnetic field, and  $\gamma = (1 - \beta^2)^{-0.5}$  the Lorentz factor.

It is important to note that the equation for the absorption coefficient has the same properties as the equation for the growth rate since the growth rate is

$$\Gamma_\pm = -k_\pm \cdot v_g \quad (15)$$

where  $v_g$  is the group velocity given by (Melrose 1989)

$$v_g = \frac{\partial \omega}{\partial k} = \frac{c}{\frac{\partial(\omega n_{ref})}{\partial \omega}} \left( \hat{k} - \frac{L_\sigma T_\sigma}{1 + T_\sigma^2} \mathbf{t} \right) \quad (16)$$

As in all previous studies, we neglected the angle between

the group velocity and the wave vector. The group velocity in our study is therefore assumed to be in direction  $\hat{k}$ , and of magnitude

$$v_g = \frac{c}{\frac{\partial(\omega n_{\text{ref}})}{\partial\omega}} \quad (17)$$

In this work we assumed the power-law electrons have a power-law dependence on kinetic energy

$$u(\gamma) = n_{\text{hot}} \cdot (\delta - 1) \cdot (\gamma_{\min} - 1)^{\delta-1} \cdot (\gamma - 1)^{-\delta} \quad (18)$$

where  $n_{\text{hot}}$  is the number density of the fast electrons, and the power law starts from a low-energy cut-off  $\gamma_{\min}$  and ends at a high-energy cut-off  $\gamma_{\max}$ . The distribution is normalized to  $n_{\text{hot}}$  when we neglect  $(\gamma_{\min} - 1)/(\gamma_{\max} - 1)$ . For the ambient plasma we used a thermal distribution (Lang 1980)

$$u(\gamma)d\gamma = n_{\text{cold}} \frac{2}{\sqrt{\pi}} \left( \frac{mc^2}{kT} \right)^{3/2} \sqrt{\gamma - 1} \times e^{-\frac{mc^2}{kT}(\gamma-1)} d\gamma \quad (19)$$

where  $n_{\text{cold}}$  is the number density of the cold, ambient plasma, electrons.

For the pitch angle dependence in the fast distribution we used an ideal loss-cone (Melrose & Dulk 1982)

$$g(\phi) = \begin{cases} \text{Const.}, & \cos(\phi) < \cos(\alpha) \\ \text{Const.} * \frac{\cos(\alpha - \Delta\alpha) - \cos(\phi)}{\cos(\alpha - \Delta\alpha) - \cos(\alpha)}, & \cos(\alpha) < \cos(\phi) < \cos(\alpha - \Delta\alpha) \\ 0, & \cos(\alpha - \Delta\alpha) < \cos(\phi) \end{cases} \quad (20)$$

This describes an isotropic distribution for pitch angles above some  $\alpha$ , no electrons below another angle  $\alpha - \Delta\alpha$ , and a linear in  $\cos(\phi)$  decrease within the  $\Delta\alpha$  interval. The normalizing constant in  $g(\phi)$  depends on the loss cone parameters. For an idealized loss cone as above it is  $\text{Constant} = 1/\pi/(2 + \cos(\alpha) + \cos(\alpha - \Delta\alpha))$ . With this definition the integral is normalized so that  $2\pi \int_{-1}^1 g(\phi)d(\cos\phi) = 1$ .

For the thermal plasma the distribution is isotropic and therefore  $g(\phi) = 1/4/\pi$ .

### 3 OTHER PROCESSES

There are other processes in a thermal plasma which have to be taken into account. The free-free absorption coefficient for  $T > 3 \cdot 10^5$  K is (Lang 1980)

$$k_{\text{ff}} = 0.01 \frac{n_e^2}{\nu^2 T^{3/2}} \left( 24.57 + \ln \frac{T}{\nu} \right) \quad (21)$$

where  $n_e$  is the density of the thermal electrons in  $\text{cm}^{-3}$ ,  $\nu$  the frequency of the absorbed radiation in Hz, and  $k_{\text{ff}}$  the absorption coefficient in  $\text{cm}^{-1}$ .

Our assumed number density is of order  $n_e \leq 10^{11}$ , our standard temperatures are of order  $T \approx 10^7$ , and the emission frequency for our standard values is of order  $\nu \approx 1\text{GHz}$ . The free-free absorption for these values is  $k_{\text{ff}} \approx 5 \cdot 10^{-8}$ . For a standard number of fast electrons of order  $n_{\text{hot}} \approx 10^6 \text{ cm}^{-3}$  the free-free absorption normalized to one electron is  $k_{\text{ff}}/n_{\text{hot}} < 5 \cdot 10^{-14}$ , which is negligible compared to the gyrosynchrotron absorption of the dominant modes.

The deflection time for a particle in a thermal plasma, with a particle velocity much higher than the thermal velocity but still non-relativistic, is (Benz 1993)

$$t_d = 3 \cdot 10^{-20} \frac{v^3}{n_e} \quad (22)$$

where  $v$  is the particle velocity, and  $t_d$  is the time for a deflection of 90 degrees.

Taking an electron with  $\gamma = 1.02$ , which is the low energy cutoff of our fast electron distribution, the deflection time is  $t_d \approx 62 \text{ msec}$ . The time for a deflection of only a few degrees is much shorter, but the timescale of saturation is a few milliseconds, and therefore the deflection should not be an important factor (Aschwanden 1990b). Faster particles have even longer deflection times, and are even less affected.

### 4 CONDITIONS FOR MASER AND SATURATION LENGTH

Inspection of equation 11 shows that the absorption for a distribution which is isotropic in pitch angle is negative only if the slope of  $u(\gamma)/\gamma^2/\beta$  is positive. This is the equivalent of an increase of the fast particles with energy, a distribution which is not likely to occur. The other possibility for amplification is when the distribution is not isotropic in pitch angle. In that case if the derivative of  $g(\phi)$  is large enough, and there are solutions such that the pitch angle dependent term in equation 11 is negative, then the absorption will be negative. One such distribution is the loss-cone distribution, which we use. The loss-cone distribution arises naturally in a solar flare where the magnetic field and the density increase with decreasing height from the corona to the chromosphere, and we expect a loss cone to appear near the foot-points of a flare.

A numerical computation of equation 11 with a loss-cone (equation 20) and a power-law (equation 18) results in negative absorption coefficients for several frequencies and angles to the magnetic field. Waves of these frequencies, and propagating with these angles, are amplified, and this is the Electron-Cyclotron-Maser mechanism.

The major factor determining which mode is the most important, or dominant, is  $k \times L$ , or  $\Gamma \times L/v_g$ , where  $L$  is the length of amplification (Benz 1993). If  $L$  is determined by homogeneity length-scales in the loop then the mode with largest absolute value negative absorption is dominant. However, if the maser stops operating after a distance smaller than the homogeneity scales of the loop, the amplification length is intrinsic to the ECM itself. Our goal was to derive the absorption coefficients, and the length of amplification  $L$ .

The intrinsic length of the maser was estimated with a model for the evolution of the fast electron distribution. We assumed the electrons are accelerated for a short time at the loop top, so that a pulse of fast electrons with a duration of a few milliseconds to a few hundred milliseconds is produced. The fast electrons reach an abrupt increase in the magnetic field, and the electrons with large pitch angles are reflected back. We assumed that before reaching the mirror the fast electron distribution is isotropic in pitch angle, and that all the electrons below a critical pitch angle pass the field increase. These assumptions result in the ideal loss cone distribution described by equation 20 with a loss-cone opening angle of  $\alpha$ . Our evolution model therefore began with an ideal loss-cone distribution over some volume, and at time  $t = 0$  the maser is “turned on“. We then assumed that the

anisotropic loss-cone distribution relaxes into a new distribution via the maser, and for simplicity we assumed the new distribution is also an ideal loss cone. The new distribution has a smaller opening angle  $\alpha'$ , and a power law in energy of the same power index as the original distribution. If the dominant process which causes the relaxation is the maser, the difference in energy between the initial loss-cone distribution and the final distribution is the energy available to the maser.

A useful measure of the amplification process is the *saturation length*,  $l_{\text{sat}}$ . We define the saturation length as the distance a wave can be amplified before the loss-cone distribution is relaxed so that the loss cone disappears, or the particular wave is no longer amplified. Complete relaxation for a volume element occurs when the energy in the element is reduced from the anisotropic distribution level to the isotropic distribution level. Our method for calculating the saturation length assumes that the greatest possible amplification is when the entire energy difference between initial and final loss-cone configurations is turned into maser radiation. We estimate this energy difference by assuming that the relaxation process leaves the number of fast electrons and the total parallel momentum unchanged. The length of amplification can not be larger than the smallest saturation length, and therefore if  $l_{\text{sat}}$  is smaller than the loop length-scales it determines the dominant mode. The mode with the smallest saturation length is therefore the dominant mode.

We followed the gradual closing of the loss cone in detail for some test cases, and our results justify an all-or-nothing approximation. In this approximation we assume that the distribution remains unchanged until the energy radiated by the maser is equivalent to some per cent of the kinetic energy, and then the relaxation to the lower energy configuration is instantaneous. When the closing of the loss-cone is followed it is found that the loss-cone opening angle is usually changed only by a few degrees before the absorption coefficient for the mode which had the largest amplification becomes positive. However, this happens after a distance which is only larger by 20 to a 100 per cent of the  $l_{\text{sat}}$  calculated with the all-or-nothing approximation, when we assume the energy turned into the maser is 10 per cent of the kinetic energy. The energy difference with the gradual closing method is usually 7–10 per cent of the total kinetic energy. Our all-or-nothing method is simple and gives a transparent relation between the absorption and the saturation length.

Our calculations are predicated upon the assumptions that the magnetic field strength  $B$ , the direction to the observer  $\theta$ , and the densities  $n_{\text{cold}}, n_{\text{hot}}$  are constant. Figures 3, 4, and 5 show contours of negative absorption coefficients around the area of maximum negative absorption. From these figures it is evident that a change in direction of the magnetic field by even  $1^\circ$  removes a propagating wave from the peak of negative absorption. Likewise a change of 1 per cent in the magnetic field makes the normalized frequency  $\nu/\nu_B$  of a wave change by about 1 per cent, and also removes the wave from the peak of amplification. Estimates of the scale lengths for the magnetic field are usually such that changes of 1 per cent occur over distances of about  $L = 10^7$  cm (Aschwanden & Benz 1988). Therefore, for saturation lengths much larger than  $10^7$  cm, we expect the amplification ceases before the particular wave reaches its saturation

length, and the loss-cone either persists through the loop, or perhaps relaxes by some other means.

#### 4.1 Energy in the Loss-Cone

The total momentum parallel to the magnetic field for a one-sided loss cone distribution with constant density in angle up to  $\cos(\phi) = \cos(\alpha)$  and no electrons for higher  $\cos(\phi)$ , and with power law in kinetic energy is

$$\begin{aligned} P_{||} &= \int_{\gamma_{\min}}^{\gamma_{\max}} \int_{\phi=0}^{\phi=\pi/2} d\gamma d(\cos(\phi)) m \gamma \beta c \cos(\phi) 2\pi u(\gamma) g(\phi) = \\ &= \frac{mc}{2\pi(1+\cos(\alpha))} \frac{\cos^2(\alpha)}{2} W_{\gamma} \end{aligned} \quad (23)$$

Where the dependence on energy is included in the integral

$$W_{\gamma} = n_{\text{hot}}(\delta - 1)(\gamma_{\min} - 1)^{\delta-1} \int \sqrt{\gamma^2 - 1}(\gamma - 1)^{-\delta} d\gamma \quad (24)$$

and  $\gamma_{\min}$  is the lowest energy,  $\gamma_{\max}$  the highest energy, of the fast electrons.

The dependence on the opening angle of the loss-cone  $\alpha$  is included in the first part of the formula for  $P_{||}$ , where the integral over  $\phi$  was done on the positive side of the distribution,  $\phi \leq 90^\circ$ , and where we assume the transition zone from isotropic distribution to the empty region is negligible.

The energy dependent integral  $W_{\gamma}$  is especially simple for the case of a power law in energy with  $\delta = 3$  and is

$$W_{\gamma} = \frac{2n_{\text{hot}}}{3} (1 + \gamma_{\min})^{3/2} (\gamma_{\min} - 1)^{1/2} \quad (25)$$

where we have neglected, as is usually done, terms of order  $(\gamma_{\min} - 1)/(\gamma_{\max} - 1)$ . We use  $\gamma_{\min} = 1.02$  and  $\gamma_{\max} \geq 3$  in our calculations.

We also need the equation for the kinetic energy density in a power law distribution which is

$$E_k = \frac{\delta - 1}{\delta - 2} mc^2 n_{\text{hot}} (\gamma_{\min} - 1) [\text{erg cm}^{-3}] \quad (26)$$

where  $n_{\text{hot}}$  is the number density of fast electrons.

We demand conservation of parallel momentum when the distribution changes from a loss-cone with opening angle  $\alpha$  and  $\gamma_{\min}$  to a distribution with  $\gamma_{\min}'$  and  $\alpha'$ , so that  $P_{||}(\cos(\alpha), \gamma_{\min}) = P_{||}(\cos(\alpha'), \gamma_{\min}')$ . From the parallel momentum conservation condition, and given  $\cos(\alpha), \gamma_{\min}, \cos(\alpha')$ , we calculate  $\gamma_{\min}'$ . From  $\gamma_{\min}'$  and equation 26 we calculate the amount of energy lost in the transition from a loss cone with  $\alpha$  to a loss cone with opening angle  $\alpha'$ . The transition to a lower cut off energy is physically reasonable since we expect electrons with low  $\gamma$  to emit in the low frequencies more than electrons with high  $\gamma$ , and when these electrons lose energy they move to smaller  $\gamma$ -es.

As an example we took an initial distribution with  $\cos(\alpha) = 0.8, \gamma_{\min} = 1.02$ , which is similar to our standard loss-cone. From equations 23 to 25 the isotropic distribution ( $\cos(\alpha') = 1$ ) which has the same total parallel momentum is a distribution with  $\gamma_{\min}' = 1.01026$ . Therefore, about fifty per cent of the energy was lost in the transition from a loss-cone with  $\cos(\alpha) = 0.8$  and  $(\gamma_{\min} - 1) = 0.02$ , to an isotropic distribution with  $\cos(\alpha') = 1$  and  $(\gamma_{\min}' - 1) = 0.01026$ . An estimate of fifty per cent is two orders of magnitude larger

than that found by Mackinnon, Vlahos & Vilmer (1992) who estimated the energy as 1 per cent of total kinetic energy, and one order of magnitude larger than that given by White, Melrose & Dulk (1986). However, this estimate is about the same as quoted by White et.al. (1986) as resulting from analytic arguments.

We also expect that a particular wave is no longer amplified once the loss cone characteristics have changed even slightly. Therefore we should have calculated the energy loss when the loss cone angle changed from  $\cos(\alpha) = 0.8$  to, say,  $\cos(\alpha) = 0.82$ . The energy loss for this case turns out to be only seven (7) per cent. Since our purpose was merely to get an estimate for the energy available to the maser, we can take as a reasonable estimate ten per cent of the kinetic energy. The exact number has very little effect on the saturation length, but the brightness temperature is directly proportional to the energy (see equation 39).

## 4.2 Saturation Length

To calculate the saturation length from the energy estimated to be available to the maser we assume that the maser is dominated by one mode ( $\nu, \theta$ ). We assume that the entire energy is concentrated in this one frequency and direction, with a typical angular width according to our numerical computations of  $\Delta\Omega = 0.1 \pi$ , and a typical frequency width of  $\Delta\nu = 0.015\nu_B$ .

To decide which is the most important mode we used the typical frequency and angular widths, calculated the saturation length for every mode as if that mode was the dominant one, and then compared saturation lengths. Usually the mode with the largest absolute value absorption coefficient also has the smallest saturation length, and is therefore the dominant mode.

A justification of this approach is seen for example in Fig. 3. The figure shows contours of equal absorption coefficient for the case  $\nu_p/\nu_B = 1, T = 5 \cdot 10^6$ , and the OM. The absorption coefficients are negative, and therefore the figure shows equal amplification contours. The maximum amplification in Fig. 3 is in the region  $0.795 < \cos(\theta) < 0.8$  and  $1.04 < \nu/\nu_B < 1.045$ . If the magnetic field strength decreases by one per cent the frequency of the wave moves from approximately  $1.04\nu_B$  to approximately  $1.05\nu_B$ , and the amplification is decreased by approximately half. Likewise, if the inclination of the field changes by one degree, the amplification is also reduced by approximately half. It is therefore justified to use narrow frequency and angular widths.

The simplest method of calculating the saturation length is the all-or-nothing method. The amplification of any mode is calculated from the length over which there is negative absorption, which is assumed to be arbitrary at first. On the other hand the intensity produced from a given volume must be limited by the total energy in the volume. The length for which the loss cone persists is calculated self-consistently by equating the energy in the wave, and the energy in the volume.

The total power of the maser per unit area is

$$P = I(\nu, \cos(\theta)) \Delta\Omega \Delta\nu \quad (27)$$

The energy increases over a volume equal to the path of

amplification times unit area, and therefore the total energy available to the maser is

$$0.1 \times E_k \times l_{\text{sat}} \quad [\text{erg cm}^{-2}] \quad (28)$$

where we used section 4.1 and our estimate of 10 per cent of the total kinetic energy as the energy available to the maser, and  $l_{\text{sat}}$  is the length of amplification – which is unknown as yet.

Assuming that the maser lasts for a given time  $\Delta t$ , and that the intensity of the emission is constant for that time, the equation which has to be solved is

$$P\Delta t = 0.1 \times E_k \times l_{\text{sat}} \quad (29)$$

By using the radiation transfer equation for negative absorption

$$I = \frac{j}{k} (1 - e^{-kx}) \approx \frac{j}{|k|} e^{|k|x} \quad (30)$$

where we have neglected 1 compared to the exponent, and assumed that  $j, k$  are constant everywhere, we have

$$\frac{j}{|k|} e^{n_{\text{hot}}|k|l_{\text{sat}}} \Delta\Omega \Delta\nu \Delta t = 0.1 \times 2 \times 8.2 \cdot 10^{-7} \times n_{\text{hot}} \times (\gamma_{\text{min}} - 1) \times l_{\text{sat}} \quad (31)$$

where we used equation 26 with  $\delta = 3$ , and also introduced normalized (to 1 particle) absorption and emission coefficients.

If we assume the maser lasts for a given time  $\Delta t$  the equation can be solved numerically for any  $\Delta t$ . However, if we assume  $\Delta t = l_{\text{sat}}/v_g$ , with  $v_g$  given by equation 16, then the solution is straightforward, and the result of the simple method is

$$l_{\text{sat}} = \ln \left( \frac{0.1 \cdot E_k \cdot v_g \cdot |k|}{\Delta\Omega \Delta\nu \cdot j} \right) / (n_{\text{hot}}|k|) \quad (32)$$

A more complicated method of deriving the saturation length is the differential approach. We assume a loss-cone distribution over some volume of space. We further assume that the maser is “turned on” at time  $t = 0$ . The intensity at time  $t$  arriving into a volume element is given by equation 30 with  $x = v_g t$ , since a wave starting at time  $t = 0$  has advanced this distance by time  $t$ . A volume element adds to the intensity a fractional intensity

$$dI = (j - kI)dx \quad (33)$$

and again neglecting 1 compared to the exponent, the intensity increase for a volume element is

$$\frac{dI}{dx} \approx |k|I \approx j e^{|k|v_g t} \quad (34)$$

The power in  $\text{erg s}^{-1}$  drawn from a unit volume at time  $t$  after the maser was turned on, assuming that  $k$  and  $j$  remain independent of  $t$  and the same everywhere, is therefore:

$$\Delta P(t) \approx \int d\Omega \int d\nu j e^{|k|v_g t} \quad (35)$$

The energy drawn from from a unit volume from time  $t_1$  to time  $t_2$  is

$$\Delta E = \int_{t_1}^{t_2} \Delta P(t) dt \approx \int d\Omega \int d\nu \frac{j}{|k|v_g} (e^{|k|v_g t_2} - e^{|k|v_g t_1}) \quad (36)$$

Since energy is being drawn from the volume element the distribution function changes, and here we use section 4.1. We assume that the distribution changes so that it remains a power-law with index  $\delta$  in energy, and a loss-cone. The new distribution function, with less energy, has a new and smaller  $\gamma_{\min}'$  and a new and larger  $\cos(\alpha')$ . From our calculated energy loss for some interval  $t_2 - t_1$  we write  $E'_k = E_k - \Delta E$ , and derive  $\gamma'$ . From the condition that the parallel momentum is constant  $P_{\parallel}' = P_{\parallel}$ , and using  $\gamma'$ , we derive  $\alpha'$ . We can then calculate the new absorption and emission coefficient, the new energy loss, and so on, and repeat the process iteratively. If we take  $t_1 = 0$  and  $t_2 = \tau = l_{\text{sat}}/v_g$ , and substitute for the integrals the constants  $\Delta\Omega$  and  $\Delta\nu$ , the equation for the saturation length we derive from the differential approach is identical to the equation of our simple method (equation 32).

We followed the gradual closing of the loss-cone iteratively for a few test cases. We took into account the change of the absorption and emission coefficients for waves arriving in later times, which passed through regions where the distribution has already changed. The results of this method are that about 3–7 per cent of the kinetic energy is turned into maser radiation, mostly in the dominant mode, that this happens after a time  $< 2 \cdot \tau$ , and that the intensity of the maser is very near to the intensity after amplification with the original maximum absorption over length  $l_{\text{sat}} = \tau v_g$ . Thus the natural growth time of the maser to maximum is  $\leq 2\tau$  and the length over which maser amplification is possible is  $\leq 2v_g\tau$ , and our simple method is a very good approximation.

Since the results of following the closing of the loss-cone and just assuming a fixed energy available to the maser are so close, we used for the rest of our calculations a fixed 10 per cent energy availability. The results given in this work were calculated with this assumption.

## 5 CALCULATIONS

Our calculations were carried out within the frame of the cold-plasma and the magneto-ionic approximations (Melrose 1989). We therefore disregard any negative absorption for frequencies which do not obey either of the two cold-plasma criteria 9 and 10, where “much larger” in these criteria is taken to be at least 10 times larger.

We calculated the absorption coefficient with equation 11, and the emission coefficient with the equation appropriate for it (Ramaty 1969). We performed the calculation using a power-law distribution in equation 11 to get the absorption due to the fast electrons, and also using a thermal distribution in the equation to get the absorption due to the ambient plasma, and the absorptions were then added to derive the total absorption. The total emissivity was derived in the same manner. The calculations were carried out without any approximations to the Bessel functions, and the full sum over the  $s$  values was performed. The integral over the pitch angle  $\phi$  was performed using the fully relativistic resonance condition 12, and the distribution functions  $f(\mathbf{p})$  were normalized to the number density of the fast electrons for the power law, and the ambient plasma for the thermal distribution. The parameters used for the calculation were

- $\delta = 3$  ;

- $\gamma_{\min} = 1.02$  ;
- $\gamma_{\max} = 3$  ;
- $\cos(\alpha) = 0.81$  ;
- $\cos(\alpha - \Delta\alpha) = 0.83$  ;
- $B = 360$  gauss ;
- $n_{\text{cold}}/n_{\text{hot}} = 10^4$ , unless otherwise indicated ;
- The ambient density is taken to be  $n_{\text{cold}} = 1.24 \cdot 10^{10} (\nu_p/\nu_B)^2 \text{ cm}^{-3}$ , which gives  $\nu_p = 1 \text{ GHz}$  for  $\nu_p/\nu_B = 1$ .

We used  $\gamma_{\max} = 3$  because several tests we performed showed that electrons with higher kinetic energy do not contribute to emission in the frequencies of the maser.

For every given pair of  $(\nu_p/\nu_B, T)$  we calculated the absorption and emission coefficients on a grid of  $\cos(\theta) = 0.02 - 0.92$ , with a spacing of  $\Delta\cos(\theta) = 0.02$ . For every  $\cos(\theta)$  we calculated the coefficients for the frequency range from  $\nu = \nu_B$  to  $\nu = 3\nu_B$ , or higher if required, and with a changing resolution. The initial scanning resolution was changed from  $\Delta\nu/\nu_B = 10^{-4}$  for the small  $\cos(\theta)$  to  $\Delta\nu/\nu_B = 0.01$  for the larger  $\cos(\theta)$ . When negative absorption coefficients were found the resolution was increased ten fold, and the calculation for the range where the absorption is negative was performed with the higher resolution. In this way we are confident that no negative absorption in the  $(\cos(\theta), \nu)$  range was missed. Sometimes calculation was performed with better resolution in  $\Delta\cos(\theta)$  or  $\Delta\nu/\nu_B$  if the absorption coefficients changed too much with the coarser resolutions. We performed calculations for the entire range  $\nu_p/\nu_B = 0.1 - 3$ , but present only examples.

Negative absorption appeared for the OM and XO near the harmonics of the cyclotron frequency, and for the ZM also near the upper hybrid frequency. Therefore it was usually not necessary to search the whole range  $\nu_B - 2\nu_B$  and the whole range  $2\nu_B - 3\nu_B$  to find the negative coefficients.

Calculation of the saturation length was performed as described in the section *Saturation Length*, with the assumption of constant width in angle and frequency. The widths enter the saturation length only logarithmically, so the result is only weakly dependent on them. Typical numbers are  $\Delta\Omega = 0.1\pi$  and  $\Delta\nu = 0.015\nu_B$ .

The tables summarizing our results are arranged according to  $\nu_p/\nu_B$ . Every row gives the characteristics of the most important wave for the given mode and temperature, and for the  $\nu_p/\nu_B$  of the table. The waves are either those with the largest (in absolute value) absorption coefficient, or those with largest growth rate, for all  $\theta$  and  $\nu$ . The first column is the temperature used to calculate the absorption coefficient for the ambient plasma, in units of  $10^6 \text{ K}$ . The temperature affects only the thermal absorption and not the absorption calculated from the power law electrons. The second column is the frequency in units of the cyclotron frequency  $\nu_B$ . The third column is the emission angle to the magnetic field, or the angle of the wave vector  $\mathbf{k}$  (assumed to be in the  $(x, z)$  plane) to the z-axis ( $\mathbf{B}$  was assumed to be in the  $z$  direction). The fourth column gives the absorption coefficient itself, normalized to a number density of the fast particles of 1, and given for a magnetic field of 360 gauss which gives  $\nu_B = 1 \text{ GHz}$ . The absorption coefficient is therefore  $n_{\text{hot}}$  times the  $k$  which is given in the table. The fifth column is the saturation length in units of  $10^6 \text{ cm}$ , computed with our formula 32, and the assumption that  $n_{\text{hot}} = 1.24 \cdot 10^6 (\nu_p/\nu_B)^2 \text{ cm}^{-3}$ . The sixth column is

the group velocity, the seventh is the growth rate, and the last column gives the mode for which these parameters were computed.

The contour figures show only negative absorption contours, multiplied by a factor of  $-10^{12}$  to make the numbers easier to display. These are examples showing only the region of  $(\cos(\theta), \nu/\nu_B)$  plane around the largest in absolute magnitude negative absorption coefficient for some mode.

## 6 OBSERVABILITY OF THE MASER

A previous study which used a power law in energy for the fast electrons found that the ZM dominates for all  $\nu_p/\nu_B > 0.5$  (Fleishman & Yastrebov 1994b), and therefore concluded that the emission must come from regions with smaller  $\nu_p$ . Another study also concluded that the maser must come from a region of low density  $\nu_p/\nu_B < 0.25$ , because for higher densities the dominant modes reach saturation much faster than the observed durations of MW spikes (Aschwanden 1990b).

We found that for  $\nu_p/\nu_B < 1.1$ , and  $\nu_p/\nu_B > 1.8$  the ZM has the largest in absolute value negative absorption (see Fig. 1), but has the largest growth rate only for  $\nu_p/\nu_B < 0.6$  (Fig. 2). If the pulse of fast electrons has a much longer duration than the time scale of maser saturation the important factor is not the growth rate, but the saturation length. At a time after the maser saturates, the mode with the smallest saturation length has closed the loss-cone beyond its own saturation length, and therefore the smallest saturation length becomes the amplification length for all modes. Modes with longer saturation lengths can reach only a fraction of the full amplification possible to them, being amplified by a factor  $\exp(|k| \cdot L)$ , with  $L$  the saturation length of the mode with the smallest saturation length, and not  $\exp(|k| \cdot l_{\text{sat}})$ , with  $l_{\text{sat}}$  the saturation length of the mode which is  $L < l_{\text{sat}}$ . Therefore what is required is to derive the saturation length for all modes, and find the mode with the smallest saturation length. Since the saturation length is inversely proportional to the absorption coefficient, the mode with smallest saturation length is usually the mode with the largest (in absolute value) negative absorption coefficient.

These findings present a problem in that we expect a loss-cone distribution to appear near the foot-points of flare loops where the magnetic field and the density increase sharply. The cyclotron frequency-plasma frequency ratio for the footpoints is probably in the range  $\nu_p/\nu_B \approx 0.5 - 3$ , if we take as typical  $n_{\text{cold}} \approx 10^{10} - 10^{11} \text{ cm}^{-3}$  for the density of ambient plasma (Aschwanden & Benz 1997), and  $B \approx$  a few times 100 gauss as typical for the magnetic field. These values are in the range where our calculations, and previous work, predict the unobservable ZM is the dominant mode. The high amplification of the ZM would therefore seem to preclude the ECM mechanism as the producer of observable MW spikes, except in the range  $1.1 < \nu_p/\nu_B < 1.8$ .

We have, however, to consider the ambient thermal plasma at the foot points, which we assume to be at a temperature of order  $10^7 \text{ K}$ . The thermal effect was not taken into account in most studies, and those which did – assumed much lower temperatures for the ambient plasma than we do. We use the range of temperatures inferred from SXR observations, since we assume the model of a hot dense plasma,

heated by the fast electrons, flowing upwards to fill the loop, and emission where the fast electrons intersect the evaporation front (Aschwanden & Benz 1997).

The temperature has two effects on our results. The first is to increase the positive absorption near the harmonics of the cyclotron frequency. If the frequency where the fast electrons create negative absorption is close to a harmonic, the thermal plasma absorption decreases the amplification, or even turns the negative coefficient positive. For the XO and OM this may eliminate the amplification at a low harmonic, but these modes appear in higher harmonics and usually have negative absorption for the higher harmonics as well. The ZM is limited to frequencies less than the upper-hybrid frequency, and therefore it is possible that the introduction of high temperatures will eliminate the ZM negative absorption while leaving higher frequency OM and XO negative absorptions. The second, and more important, consideration high temperatures introduce is the cold plasma conditions. For a temperature of  $10^6 \text{ K}$  these criteria are valid for frequencies very close to the harmonics, and for very large refraction indices. However, the high temperature we assumed forced us to reject certain negative absorption results as not valid within the framework of our assumptions. We assumed that if there is any amplification for these cases it is orders of magnitude smaller than the cold plasma result, and therefore negligible. This is supported by the known effect of thermal corrections, which is to decrease the refraction indice and the absorption (Melrose 1989).

Even if the thermal positive contribution leaves a negative ZM absorption which is valid for the cold plasma approach, and is the largest in absolute value of all negative absorptions, the OM and XO may be observable. We assumed in the previous section that the largest in absolute value negative absorption coefficient dominates, and that all the energy goes into amplifying this mode. With this assumption we derived the saturation length and the amplification for this dominant mode. This is similar to the assumption in previous studies, which give the dominant mode in some parameter region as the mode with the highest growth rate (White et.al. 1986; Aschwanden 1990a), and it is justified because of the exponential nature of the intensity. There are, however, two scenarios where modes with smaller absorption coefficients can be observed. The first scenario, presented in section 6.2, depends on the high brightness temperature of the maser. The second scenario, presented in section 6.3, depends on the slowness of the Z-mode. If the ZM is slow enough, another mode may be able to reach its full amplification before the ZM saturates, and then, for a short time until the ZM saturates, this mode can also be observed.

Finally, there is a region where the ZM does not have negative absorption. For the region  $1.5 \leq \nu_p/\nu_B \leq 1.6$  the lowest frequency for which the ZM exists is higher than  $\nu_B$  and the highest frequency for which the ZM exists is lower than  $2\nu_B$ . Negative absorption usually appears near the harmonics of the cyclotron frequency, and for the ZM frequencies with this region of  $\nu_p/\nu_B$  there are no negative absorption coefficients.

All the above considerations are summarized in Fig. 1 and in Fig. 2 giving the maximum absorption coefficients and growth rates for the modes. The coefficients are the largest in all frequencies and angles for the given  $\nu_p/\nu_B$ , wave mode, and with  $T = 5 \cdot 10^6 \text{ K}$ . The ZM does not appear for

$1.6 < \nu_p/\nu_B$  because where negative absorption reappears at  $\nu_p/\nu_B > 1.6$  the frequencies fail the cold plasma criteria. It is important to note that the largest growth rate does not necessarily occur at the same angle and frequency as the largest in absolute value negative absorption coefficient, as can be seen in Tables 1 to 6.

Whatever mode is amplified, the ECM is difficult to observe because of the narrow bandwidth, and especially because of the small angular width of the emission. Fig. 3 shows contours of negative absorption coefficients around the area where the OM has the largest negative absorption (largest in absolute value). To observe the emission it is necessary to be within a cone of less than 1 degree around the angle of maximum amplification, and within 1 per cent of the frequency of maximum amplification. The absorption 1 per cent away from the maximum drops by half, which for an exponential growth with a maximum power of the exponent of about 30 means a drop of 7 orders of magnitude in amplification. In Fig. 4 and Fig. 5 the same narrow bandwidth and small angular width are seen for the other modes, and the phenomena occurs for all other  $\nu_p/\nu_B$  values. This general result means that observation of ECM should be rare, even if ECM is very common and occurs at all times.

### 6.1 Thermal Effect

In most cases the thermal plasma tends to suppress maser emission, as was noted in previous studies (Aschwanden 1990b; Kuncic & Robinson 1993). For example for  $\nu_p/\nu_B = 0.8$  (Table 1) and  $T = 5 \cdot 10^6$  K, the most important OM was found at frequency  $\nu/\nu_B = 1.03$ . At a higher temperature of  $10^7$  K the most important OM moved to a higher frequency of  $\nu/\nu_B = 1.079$ . The fast electrons still gave the same negative absorption at  $\nu/\nu_B = 1.03$ , only for  $T = 10^7$  the thermal absorption was large enough to turn the absorption at this frequency positive. On the other hand, the ZM at  $\nu/\nu_B = 1.2745$  was not affected by the thermal absorption, because of its distance from the cyclotron frequency. The change there was the result of the application of the cold plasma criteria, which for  $T = 10^7$  this frequency violates, and therefore the largest acceptable absorption was at a lower frequency, further from the resonance and with a smaller refraction index. All these changes were not enough to change the dominant mode, which remained the ZM, because the OM absorption was reduced by a factor of 8, while the ZM absorption was reduced only by a factor of 4. The total effect of the higher temperature was therefore to reduce the relative importance of the OM emission.

The other ZM given in Table 1 is the ZM wave with the largest growth rate. This is a wave at a much lower frequency, and a slightly different angle than the wave with largest (negative) allowable absorption coefficient. This mode also changes with the increase in temperature from frequency  $\nu/\nu_B = 1.0351$  for  $T = 5 \cdot 10^6$  to frequency  $\nu/\nu_B = 1.087$  for  $T = 10^7$ . In this case the absorption was only reduced by a factor of 2, and the growth rate by about the same. This is an example where the mode with the largest growth rate is not the dominant mode.

A counter example is demonstrated in Table 6. The first row of Table 6 gives a negative absorption coefficient for the frequency  $\nu/\nu_B = 2.04885$ , which is very close to the ZM resonance for this case. The refraction index for this

frequency and for the angle  $\cos(\theta) = 0.06$  is  $n_{\text{ref}} = 4.42$ , which was large enough for this solution to barely violate the 1st plasma criterion (eq. 9), giving a value only 9.5 times larger than  $0.001683/2$ . This is not allowed, which is why the row is marked as ZMN in the table. Therefore, for  $\nu_p/\nu_B = 1.8$  the temperature leads us to discard the ZM waves as unimportant, and leaves us with the OM as the dominant mode.

When we made the calculations in Table 6 with a temperature of  $T = 10^7$  K, all the ZM negative coefficients disappeared entirely, overcome by the thermal absorption, and therefore there was no need to even consider the cold plasma criteria.

It is important to note a problem with Table 6 which is that the negative absorption coefficients are very small. The saturation lengths were therefore very large, and may violate the assumption that the maser is very small compared to the dimensions of the loop. For example for  $T = 10^7$  K the saturation length for the OM was found to be  $l_{\text{sat}} = 1.8 \cdot 10^8$  cm, which is large enough for our assumption that the magnetic field, the density, and the temperature are constant to be incorrect. In such a case the maser does not reach its saturation intensity, and the loss cone may relax by some other means.

### 6.2 Non-Dominant Mode

Since the intensity  $I$  is difficult to measure we would like to estimate the brightness temperature

$$T_B = \frac{c^2}{2\nu^2 k_B} \frac{I}{\nu/\text{GHz}} = 3.26 \cdot 10^{18} \frac{I}{(\nu/\text{GHz})^2} \quad (37)$$

We can express the intensity in terms of the saturation length, use equation 32, and write the intensity (equation 30) as

$$I = \frac{j}{|k|} \left( \frac{0.1 E_k v_g |k|}{\Delta\Omega \Delta\nu j} \right) \quad (38)$$

Using this, the brightness temperature for the dominant mode can now be written as

$$T_B = \frac{3.26 \cdot 10^{18}}{(\nu/\text{GHz})^2} \frac{0.1 E_k v_g}{\Delta\Omega \Delta\nu} \quad (39)$$

Therefore for the dominant mode the brightness temperature depends only on the mode (through  $v_g$ ) and on the energy assumed to be available to the maser, and not on the saturation length  $l_{\text{sat}}$ .

We estimated the importance of any wave with negative absorption by calculating a saturation length assuming this particular wave is the only amplified one. We then compared the various non-dominant saturation lengths to the saturation length of the dominant mode, where by definition the dominant mode is the mode with the shortest saturation length. The amplification length of a non-dominant mode is limited to the loss-cone length determined by the dominant mode  $l_{\text{dom}}$ . The intensity of the non-dominant mode can then be calculated by using the non-dominant absorption and emission coefficients with the dominant mode's saturation length. The intensity to be used in equation 37 is for this case

$$I_{\text{non}} = \frac{j_{\text{non}}}{|k_{\text{non}}|} e^{|k_{\text{non}}| \cdot l_{\text{dom}}} \quad (40)$$

or, alternatively

$$I_{\text{non}} = \frac{j_{\text{non}}}{|k_{\text{non}}|} \left( \frac{0.1 E_{\text{k}} v_{\text{g}} |k_{\text{dom}}|}{\Delta \Omega \Delta \nu j_{\text{dom}}} \right)^{k_{\text{non}}/k_{\text{dom}}} \quad (41)$$

Where  $k_{\text{dom}}, j_{\text{dom}}$  are for the dominant mode, which determines the saturation length, and  $k_{\text{non}}, j_{\text{non}}$  are for some other mode, at a different frequency and another emission angle, but which also has a negative absorption, and is therefore amplified. This formulation is true no matter which is the dominant mode, also for the ZM.

If  $|k_{\text{non}}| \cdot l_{\text{dom}}$  is large, the resulting intensity is large and observable. For example for  $\nu_{\text{p}}/\nu_{\text{B}} = 1$  (Table 2) and  $T = 5 \cdot 10^6$  K the XO saturation length was the shortest of all modes, though very close to the ZM saturation length. However, the OM absorption coefficient was also very close to the XO absorption coefficient, and obviously the non-dominant situation is relevant. This is also one of the rare cases where the OM was slower than the ZM, so the growth rate of the OM was much smaller than the growth rate of the ZM, and certainly smaller than the growth rate of the XO. In spite of that, our model predicts a strong emission in the OM for this table's  $\nu_{\text{p}}/\nu_{\text{B}} = 1$ . For this case  $j/k$  for the OM is about 1/16 of the  $j/k$  ratio for the XO. Therefore even when the power of the exponent is the same, the total intensity in the OM is only 1/16 of the intensity in the XO.

If the non-dominant mode has a much smaller absorption, for example as in  $\nu_{\text{p}}/\nu_{\text{B}} = 1$  (Table 2) and  $T = 10^7$  K, where  $k_{\text{non}} \approx k_{\text{dom}}/3$ , then the non-dominant intensity is much smaller. For example if we assume  $k_{\text{dom}} \cdot l_{\text{dom}} \approx 25-30$ , as it often is, and the same  $j/k$  for the dominant and non-dominant modes, the factor between the intensities is  $e^{17} \approx 10^7$ . This factor reduces a brightness temperature of  $10^{18}$  K to a brightness temperature of only  $10^{11}$  K, which is lost against the background of the entire loop, and is in any case much lower than is observed for microwave spikes.

The way to decide when a non-dominant mode could be observed is to compare absorption coefficients. In Fig. 2 the XO growth rate for  $\nu_{\text{p}}/\nu_{\text{B}} = 1$  (of the example above) appears to be much larger than the OM growth rate. However, in Fig. 1 we see that the absorption coefficients are equal. The example of the previous paragraph shows that the OM is observable whenever such a situation occurs.

### 6.3 Slow Mode Saturation

Another possibility for observation of a non-dominant mode is for the case of the dominant mode being slow. The Z-mode is usually a slow wave, especially near its resonance frequency, where its group velocity can be even as low as  $c/500$ . It is therefore possible that when a certain set of conditions is met another mode is amplified to its maximum. This can happen if the Z-mode is slow enough that the other mode reaches its saturation length before the ZM saturates. In that case until the ZM saturates and reduces the energy in the distribution, the other mode is emitted with the full amplification of its own saturation length.

The growth rate equation 15 already includes the group velocity, and therefore a comparison of growth rates suffices to show if this slow-mode scenario is possible. It is also possible to take the group velocity into account from the perspective of the spatial absorption coefficient, though we need

a few assumptions. We assumed a typical emitting electron energy of  $\gamma = 1.1$ , and that the important electrons are on the edge of the loss cone with pitch angle  $\cos(\phi) = 0.8$ . These parameters gave a velocity parallel to the magnetic field of  $c/3$  for the most important electrons, while the OM or XO wave was usually faster than  $c/3$ .

For an example we used Table 4 for temperature of  $10^7$  K. The OM group velocity is  $0.783 \cdot c$ , and the ZM group velocity is  $0.1253 \cdot c$ . An OM wave of speed  $0.783 c$  beginning near the mirror point at time  $t_1$  after the first electrons mirrored overtakes these first electrons (of parallel velocity  $c/3$ ) at time  $t_2 = 1.74 \cdot t_1$ , and at a point  $0.58 c \cdot t_1$  from the mirror point. In our model (section 4.2), when this distance is the saturation length,  $0.58 c \cdot t_1 = l_{\text{sat}}^{\text{OM}}$ , the intensity of the radiation is so great that the end-most volume element with a loss-cone distribution is drained of its free energy, and the loss-cone distribution disappears from that end-most volume. A Z-mode wave emitted at time  $t = 0$ , and having a group velocity of  $0.1253 c$ , has propagated by this time only to a distance of  $0.1253 \cdot c \cdot t_2 = 0.376 \cdot l_{\text{sat}}^{\text{OM}}$ . If the ZM with this group velocity has an absorption coefficient such that its saturation length is for example 0.4 of the OM saturation length, the Z-mode had not saturated by the time the OM emission has reached its peak and is beginning to close the loss-cone. However, at some later time the ZM will have had time to saturate near the mirror-point, and has closed the loss-cone close to the mirror. An OM/XO wave starting from the mirror point at that time does not see a loss-cone, and is not amplified. For the case in Table 4 the ZM has a saturation length only 0.27 of the OM saturation length, and therefore the ZM has saturated by the time the OM wave reaches its saturation length. This however does not mean that the OM is not amplified as explained below.

A better calculation than the above takes into account that the OM wave advances faster than the electrons and much faster than the ZM wave. The requirement then is that the electrons the OM wave passes have not themselves gone previously through a saturated Z-mode wave, and therefore have retained the loss-cone distribution. The result of that requirement is that for a mode with  $l_{\text{sat}}$  to be amplified, the Z-mode saturation length  $l_z$  must be large enough so that the inequality below is correct :

$$\frac{l_z}{l_{\text{sat}}} \geq \frac{v_z}{v_e} \frac{v_g - v_e}{v_g - v_z} \quad (42)$$

With  $v_e$  the velocity of the electrons,  $v_g$  the group velocity of the OM or XO,  $v_z$  the group velocity of the ZM,  $l_z$  the saturation length of the ZM,  $l_{\text{sat}}$  the saturation length of the OM. The same equation holds for any two modes, one with group velocity  $v_z$  slower than the electrons, and the other with group velocity  $v_g$  faster than the electrons.

For the case of Table 4 the left side of the equation is 0.27 while the right side is 0.257, and therefore the OM can reach its maximum possible amplification before the ZM closes the loss-cone and prevents it.

A simpler estimate for the relative importance of the modes is to compute  $\tau = l_{\text{sat}}/v_g$  for each of the modes. This estimate is very close to calculating the growth rate, since dividing the saturation length by  $v_g$  is equivalent to replacing the absorption  $k$  by the growth rate  $\Gamma = -k \cdot v_g$  in equation 32. This criterion tends to be smaller for a larger growth rate, and the smallest value is the most important.

For our example (Table 4,  $T = 10^7$ ) the 7th column of the table shows that the growth rate of the OM is larger than the growth rate of the ZM. Therefore, even though the saturation length of the OM is much larger than the saturation length of the ZM, and after the ZM saturates the OM disappears, the growth rate criterion, and our calculations above, show that the OM can be observed for a short duration, until the ZM saturates.

Another example is for  $\nu_p/\nu_B = 0.8$  (Table 1),  $T = 5 \cdot 10^6$  and the ZM. In the Table we give both the ZM wave with largest (absolute value) negative absorption, and the ZM wave with the largest growth rate. The ZM wave with the largest absorption is very slow and has a very small growth rate, and therefore the important wave is at first the one with the largest growth-rate. For  $\nu_p/\nu_B = 0.8$  the largest growth rate in the ZM is still smaller than the growth rate of the OM wave, and therefore we conclude that the OM reaches its saturation length before the ZM closes the loss-cone, and we expect to see an OM wave for a short time. It turns out that the difference between the time to saturation for the OM and the time to saturation for the largest growth rate ZM is very small, about 0.1 msec. The time we expect to see the OM at its full amplification is therefore very small.

In this case it was useful to check the non-dominant-mode approach of the previous section, and we found that the OM is observed until the small saturation length ZM saturates. When we used the OM absorption coefficient with the saturation length of the largest growth rate ZM we got a brightness temperatures of order  $T_B = 10^{15}$ , which is observable.

#### 6.4 Time Dependence

The duration of the pulse of fast electrons is obviously unrelated to the loss-cone time scales. If the pulse is shorter than the loss-cone time-scale, less than  $t_2 = 3 \cdot l_{\text{sat}}/c$  for the example of the previous section, the maser intensity in the OM is not strong enough to close the loss-cone. The loss-cone distribution therefore moves from the mirror point at the typical loss-cone velocity, and the maser continues to emit, though at a weak intensity. Using the terminology of the example from the previous section, and assuming a pulse duration of  $t_1$ , the maximum amplification length is  $c \cdot t_1/3$ . In the example we had  $l_{\text{sat}} = 0.58 \cdot c \cdot t_1$ , and therefore the maximum amplification length is about  $l_{\text{sat}}/2$ . Since the intensity is exponential with the amplification length, this translates into a much weaker emission. Typically the power of the exponent for the dominant mode is 20–30, and with  $l_{\text{sat}}/2$  the intensity is more than a hundred thousand times weaker. For such a case it is unlikely that the maser emission can be observed at all.

The other extreme is that the pulse of fast electrons persists for a time much longer than typical maser saturation times. For such a case, the loss-cone closes at distance  $l_{\text{sat}}$  from the mirror point, but new fast electrons move into place constantly. At first glance it would seem that the maser persists for approximately the duration of the pulse, however, if there is a ZM with a smaller saturation length than the observable modes this does not happen. After the Z-mode reaches its saturation length it quenches the fast electron loss-cone distribution, and the observable modes can not be amplified enough to be seen. In this picture the ZM waves

saturate and maintain an intensity just strong enough to drain every new volume element of its energy when it overtakes the ZM waves. An observable OM or XO wave starting from the mirror at a time  $t > t_1$  of the previous section, so that the ZM has already reached saturation  $t > l_{\text{sat}}^{ZM}/v_g^{ZM}$ , does not see a loss-cone, and therefore is not amplified. For our example above, the intensity of an observable mode at first increases, reaching a maximum at time  $t_2$  after the first electrons are mirrored. At this time the OM wave which left the mirror at  $t_1$  reaches  $l_{\text{sat}}$ . This high intensity can last only until OM waves leaving the mirror encounter saturated ZM waves. For the example from Table 4 the ZM reaches its saturation length near the mirror at time  $1.25 \cdot t_1$ . An OM wave leaving the mirror point at  $1.25 \cdot t_1$  reaches  $l_{\text{sat}}$  at  $t_2 + 0.25t_1$ , and the maser then starts to decrease in intensity. The maser is therefore at peak intensity only for a time  $0.25t_1 = 1.7$  msec. Of course, if the shortest saturation length is for an observable mode, the maser does persist for the length of the pulse of accelerated particles.

Our conclusion is therefore that if the smallest  $l_{\text{sat}}$  is for the ZM, the maser persists for a time less than but of order  $[l_{\text{sat}}/v_g]_{ZM}$ , regardless of the duration of the fast electron acceleration pulse. This is the case for Table 1 at all temperatures. Of course, after the pulse ends, the waves disappear, and when a new pulse reaches the mirror point, the process can start again.

An example of a different kind is for  $\nu_p/\nu_B = 1$  (Table 2) and  $T = 5 \cdot 10^6$  K. For this case the saturation length of the XO was shorter than the saturation length of the ZM, and the saturation length of the OM was not much longer. Therefore we expect the XO radiation to last, and the OM radiation to be amplified as well. For the other tables, at  $T = 5 \cdot 10^6$  the smallest saturation length was always for an observable mode, and therefore at this temperature the loss cone should always produce long lasting maser emission.

The differential approach described in section 4.2 also gives a model for the time-profile of the maser. The emission should appear as a rising exponent, and then decrease faster than an exponent, because the elements whose energy was exhausted begin to positively absorb radiation from the still amplifying elements. This picture is at odds with the characteristics observed, which were a rise as  $e^{(t^2)}$  and a decrease as an exponent (Gudel & Benz 1990). Perhaps the gaussian rise is a feature of the acceleration mechanism, for example if  $n_{\text{hot}}$  also increases with time.

## 7 COMPARISON WITH PREVIOUS WORK

We can compare our results with only one previous case (Aschwanden 1990b) where saturation lengths were estimated, and given for example for  $\nu_p/\nu_B = 0.5$  as  $l_{\text{sat}}^{ZM} = 10$  km and  $l_{\text{sat}}^{OM} = 30$  km.

We incorporated in our program Aschwanden's thermal distribution in energy and  $\sin^6(3 \times \phi)$  loss-cone. Aschwanden used the standard parameters  $T_{\text{hot}} = 10^8$  K,  $T_{\text{cold}} = 10^6$  K,  $n_{\text{cold}} = 1.25 \cdot 10^8$  cm $^{-3}$ , and  $n_{\text{hot}}/n_{\text{cold}} = 0.01$ . With the above and from the standard  $\nu_p/\nu_B = 0.1$  a magnetic field of  $B = 360$  gauss was the standard field. If the number of particles was kept constant the magnetic field for  $\nu_p/\nu_B = 0.5$  as in the example above should have been reduced to  $B = 72$  gauss.

Our calculations with Aschwanden's distribution functions gave the normalized results, with  $B = 100$  gauss and divided by  $n_{\text{hot}}$ , for the OM:  $k = -1.1 \cdot 10^{-11}$ ,  $j = 1.69 \cdot 10^{-24}$ ,  $c/v_g = 1.144$ ,  $\nu/\nu_B = 1.019$ ,  $\cos(\theta) = 0.24$  and for the ZM:  $k = -3.6 \cdot 10^{-11}$ ,  $j = 4 \cdot 10^{-23}$ ,  $c/v_g = 7.3$ ,  $\nu/\nu_B = 1.039$ ,  $\cos(\theta) = 0.2$ . Where these numbers are for the respective largest growth rate in every mode, since that was Aschwanden's criterion for the dominant wave.

Using our simple method to calculate the saturation length, and the scaling laws  $k \propto n_{\text{hot}}/B$  and  $j \propto n_{\text{hot}} \times B$ , we got  $l_{\text{sat}}^{\text{ZM}} = 4.89$  km and  $l_{\text{sat}}^{\text{OM}} = 17.9$  km. These saturation lengths are about a factor 2 smaller than Aschwanden's. We also have to take into account Aschwanden's assumption of an initial energy density equivalent to  $T_B = 10^{14}$  K. In our model the waves amplify the spontaneous emission, and the amplification is according to the radiative transfer equation 30. A typical value is  $j/k \approx 10^{-13}$  and if this is the intensity  $I$  the equation for the brightness temperature (equation 37) gives the equivalent temperature as only  $T_B = 10^7$  K. The brightness temperature reaches  $T_B = 10^{14}$  K only after the wave has been amplified by a factor of  $10^7 \approx e^{16}$ , and the comparison of the saturation lengths should be only from this stage.

The total saturation length gives a power in the exponent of about 30, therefore if we had started with a wave at  $T_B = 10^{14}$  K the saturation length would have been only half of what we calculate. The conclusion is that computing the saturation length with our method resulted in saturation lengths of a factor of 4 smaller than those calculated by Aschwanden's method. This was the result of neglecting the change in the loss-cone during the amplification of the wave, and assuming that the absorption coefficient remains constant until the wave reaches its maximum energy. The differential iterative method shows that the actual saturation length is up to twice what the simple method gives, and therefore we get a factor of about 2 back. Considering the simplicity of the equations we use, a factor of two is extremely close.

## 8 SUMMARY

We have developed a model for estimating the intensity and duration of emission through the Electron-Cyclotron-Maser (ECM) mechanism.

Observations led us to use a power law for the fast electrons, with a minimum energy of 10 keV and maximum energy of 1 MeV. This distribution is harder than the ones studied in the past (Winglee & Dulk 1986; Aschwanden 1990a).

From recent results (Aschwanden & Benz 1997) we estimate the important ratio  $\nu_p/\nu_B$  in the foot-points of flares, which is the region of interest for this study, to be in the range 0.5–3. For most of this range a loss cone in a power law distribution of electrons results in the ZM being the dominant magneto-ionic mode. The ZM is unobservable, because when a ZM wave reaches a region with a smaller plasma frequency than the plasma frequency where the wave originated, it is absorbed. Thus it seems at first glance that the maser mechanism can not produce observable emission.

We use an absorption coefficient approach, differing from previous studies which used the growth rate. Using this

approach we calculate the *saturation length* for the competing magneto-ionic modes, and show that in many cases the observable OM and XO are amplified to observable intensities.

The conditions which enable the OM and XO modes to be amplified in the presence of a ZM with much larger (in absolute magnitude) negative absorption are: first, the inclusion of an ambient thermal plasma with temperature of order  $T = 10^7$  K; second, the low group velocity of the ZM which enables a competing mode to reach its saturation before the ZM saturates; third, the high amplification of the maser, which makes even non-dominant modes observable.

Our conclusion is that in the range  $\nu_p/\nu_B = 0.5 – 1.8$  the maser mechanism can produce observable emission in the form of intense spikes with a narrow bandwidth – about one per cent of the frequency – and narrow angular width – about  $0.1\pi$  solid angle.

The examples given in the tables indicate that long duration emission in the OM and XO appears at angles of 30–60 degrees to the magnetic field, and at 3–6 per cent of the cyclotron frequency above the nearest cyclotron harmonic. This is usually the second harmonic for the OM, and always the second harmonic for the XO. We expect the long duration emission to be determined by the duration of the pulse of accelerated electrons, and the brightness temperature to be of order  $T_B = 10^{16}$  K and above.

Short duration emission appears when the OM or XO are emitted only until the ZM saturates. For these cases the saturation lengths of the OM and XO are longer than the ZM saturation length, but the ZM group velocity is smaller than the group velocity of the OM or XO. The short duration emission lasts in our model from fractions of a millisecond to a millisecond, for example for  $\nu_p/\nu_B = 0.8$  (Table 1) and a temperature of  $5 \cdot 10^6$  K, where the OM has the largest growth rate.

From the results given in Tables 2 to 6 for a temperature of  $5 \cdot 10^6$  K, we expect emission for the parameters of the tables for the duration of the accelerated electrons' pulse, and at frequency  $\nu \approx 2.06\nu_B$ . The exception is the case of  $\nu_p/\nu_B = 1$  (Table 2) where the XO emission for  $T = 5 \cdot 10^6$  K is at  $\nu/\nu_B \approx 2.06$ , and there is also OM emission of observable intensity at  $\nu/\nu_B \approx 1.03$ . We also expect long duration emission for  $\nu_p/\nu_B = 1.2$  (Table 3) and  $T = 10^7$  K. For this case  $l_{\text{sat}}^{\text{XO}} \approx l_{\text{sat}}^{\text{ZM}}$ , and therefore the XO will be amplified to observable intensities. The XO frequency is  $\nu = 2.129\nu_B$ . For the cases  $\nu_p/\nu_B = 1.6$  and  $\nu_p/\nu_B = 1.8$  (Table 5 and Table 6) and  $T = 10^7$  and  $T = 2 \cdot 10^7$ , the OM is the dominant mode, but the saturation lengths are much too large. We conclude that the loss-cone relaxes by some other means, and not through the ECM mechanism.

In summary, this study shows that the ECM produces millisecond radio spikes such as observed from the Sun. The ECM emission reproduces the frequency of the observed spikes, the bandwidth of the spikes, the source size as recently observed (Benz et al. 1996), the brightness temperature, and the duration of the spikes.

The ECM does not produce emission at two frequencies simultaneously, and therefore can not reproduce the observed bands (Krucker & Benz 1994). However, if a loss cone distribution forms independently in different regions, and the magnetic field is not the same in these regions, then ECM in several frequencies and angles can be produced. For

example in Table 2 for temperature  $T = 5 \cdot 10^6$  the XO emission is at angle 69 degrees. In Table 3 for  $T = 5 \cdot 10^6$  the XO emission is at angle 64 degrees. If two regions, one with  $\nu_p/\nu_B = 1$  and one with  $\nu_p/\nu_B = 1.2$ , emit ECM, and if the magnetic field changes direction by a few degrees between the regions, it may become possible to observe both. Since the magnetic field and the density both increase towards the foot points, the ratio between the emitted frequencies in the two regions can be larger than 1.2.

Our model also does not reproduce the reported gaussian rise time (Gudel & Benz 1990). However, if the number of fast electrons also increases with time, the rise time is a feature of the acceleration mechanism, since the emission in ECM is directly proportional to the number density of the fast electrons.

It is possible to conclude from our results that the observed frequency of the spikes should be higher at the beginning of a flare, since the hot and dense chromospheric plasma is then still close to the chromosphere, where a large magnetic field causes a large cyclotron frequency. As the flare advances, and the evaporation front propagates upwards, temperatures below increase, the unobservable ZM dominates for the larger temperatures, and the magnetic field in the region from which ECM emission is observed is smaller.

## REFERENCES

Aschwanden M.J, 1990a, A&AS, 85, 1141  
 Aschwanden M.J., 1990b, A&A, 237,512  
 Aschwanden M.J., Benz A.O. , 1988, A&A, 332,447  
 Aschwanden M.J., Benz A.O. , 1997, ApJ, 480,825  
 Benz A.O., 1986,Sol. Phys., 104, 99  
 Benz A.O., 1993, Plasma Astrophysics Kinetic Processes in Solar  
     and Stellar Coronae. Kluwer Academic Publishers  
 Benz A.O., Graham D., Isliker H., Andersson C., Koehnlein W.,  
     Mantovani F., Umana G., 1996, A&A 305, 970  
 Fleishman G.D., Yastrebov S.G., 1994a, Sol. Phys., 154, 361  
 Fleishman G.D., Yastrebov S.G., 1994b, Sol. Phys., 153, 389  
 Gudel M., Benz A.O., 1990,A&A, 231,202  
 Holman G.D., Benka S.G., 1992,ApJ, 391, 854  
 Holman G.D., Eichler D., Kundu M.R., 1980, in M.R. Kundu,  
     T.E. Gergely , eds, Proc. IAU Symp. 86, Radio Physics of the  
     Sun. Dordrecht : Reidel, p. 457  
 Kuncic Z., Robinson P.A., 1993,Sol. Phys., 145,317  
 Krucker S., Benz A.O., 1994,A&A, 285,1038  
 Lang K.R., 1980, Astrophysical Formulae 2nd Edition. Springer  
     Verlag  
 Mackinnon A. , Vlahos L., Vilmer N., 1992,A&A, 256, 2, 613  
 Melrose D.B, 1989, Instabilities in Space and Laboratory Plasma.  
     Cambridge University Press  
 Melrose D.B, Dulk G. A., 1982, ApJ, 259, 844  
 Ramaty R., 1969, ApJ , 158, 753  
 Trulsen J., Fejer J.A., 1970, J. Plas. Phys., 4,4, 825  
 White S.M, Melrose D.B., Dulk G.A., 1986, Adv. Space Res.  
     6,6,163  
 Winglee R.M.,1985, ApJ, 291,160  
 Winglee R.M, Dulk G.A., 1986,Sol. Phys., 104,93  
 Wu C.S., Lee L.C, 1979, ApJ, 230,621  
 Zirin H., 1989, Astrophysics of the Sun. Cambridge University  
     Press

**Table 1.**  $\nu_p/\nu_B = 0.8$ 

$T/10^6$ Kelvin	$\nu/\nu_B$	emission angle Degrees	$k_{\max}$ cm $^2$	$l_{\text{sat}}/10^6$ cm	$v_g$ cms $^{-1}$	$\Gamma$ cm $^3$ s $^{-1}$	Mode
5	1.2745	82	-2.63E-10	0.064883	2.05E+07	5.37E-03	ZM
5	1.0351	75	-1.8E-11	1.947	1.13E+10	0.204	ZM
5	1.03	64	-1.34E-11	2.788	1.89E+10	0.253	OM
5	2.0616	70	-7.67E-12	4.57	2.4E+10	0.184	XO
10	1.2709	81	-6.68E-11	0.28	5.25E+07	3.5E-03	ZM
10	1.087	69	-1.01E-11	3.26	7.89E+09	0.08	ZM
10	1.079	52	-1.71E-12	21	2.11E+10	0.036	OM
10	2.131	61	-1.12E-12	29.7	2.45E+10	0.027	XO
20	1.2663	80	-4.23E-11	0.519	1.08E+08	4.6E-03	ZM
20	1.2121	70	-1.54E-11	1.801	1.38E+09	0.02	ZM
20	1.189	37	-8.48E-14	400.9	2.52E+10	2.1E-03	OM

**Table 2.**  $\nu_p/\nu_B = 1$ 

$T/10^6$ Kelvin	$\nu/\nu_B$	emission angle Degrees	$k_{\max}$ cm $^2$	$l_{\text{sat}}/10^6$ cm	$v_g$ cms $^{-1}$	$\Gamma$ cm $^3$ s $^{-1}$	Mode
5	1.036	72	-7.76E-12	2.99	1.35E+10	0.105	ZM
5	1.0301	38	-7.66E-12	3.16	5.14E+09	0.039	OM
5	2.057	69	-7.75E-12	2.98	1.99E+10	0.154	XO
10	1.0909	64	-4.05E-12	5.44	1.1E+10	0.044	ZM
10	1.076	35	-1.39E-12	16.54	9.86E+09	0.014	OM
20	1.3265	66	-3.9E-12	4.34	1.4E+09	5.5E-03	ZM
20	1.1872	26	-4.47E-14	492.6	2.09E+10	9.37E-04	OM

**Table 3.**  $\nu_p/\nu_B = 1.2$ 

$T/10^6$ Kelvin	$\nu/\nu_B$	emission angle Degrees	$k_{\max}$ cm $^2$	$l_{\text{sat}}/10^6$ cm	$v_g$ cms $^{-1}$	$\Gamma$ cm $^3$ s $^{-1}$	Mode
5	1.208	47	-1E-12	14.7	7.89E+09	7.9E-03	ZM
5	2.061	69	-5.7E-13	28.5	2.48E+10	0.014	OM
5	2.06	64	-7.9E-12	2.05	1.4E+10	0.111	XO
5	1.9653	89	-4.2E-12	3.9	7.8E+09	0.0323	XO
10	1.286	50	-1.08E-12	12.8	5.8E+09	6.2E-03	ZM
10	2.129	52	-1.08E-12	14.33	1.57E+10	0.017	XO
20	1.286	50	-1.08E-12	12.8	5.8E+09	6.2E-03	ZM
20	2.319	33	-7.65E-14	190	1.9E+10	1.45E-03	XO

**Table 4.**  $\nu_p/\nu_B = 1.4$ 

$T/10^6$ Kelvin	$\nu/\nu_B$	emission angle Degrees	$k_{\max}$ cm $^2$	$l_{\text{sat}}/10^6$ cm	$v_g$ cms $^{-1}$	$\Gamma$ cm $^3$ s $^{-1}$	Mode
5	1.422	37	-3E-13	32.3	3.76E+9	1.1E-03	ZM
5	2.0597	67	-4.3E-13	27.9	2.2E+10	9.7E-03	OM
5	2.056	31	-1.5E-12	8.5	6.4E+9	9.3E-03	XO
10	1.42	37	-3E-13	32.3	3.76E+9	1.1E-03	ZM
10	2.13	58	-9.7E-14	119.8	2.35E+10	2.3E-03	OM
20	1.42	37	-3E-13	32.3	3.76E+9	1.1E-03	ZM

**Table 5.**  $\nu_p/\nu_B = 1.6$ 

$T/10^6$ Kelvin	$\nu/\nu_B$	emission angle Degrees	$k_{\max}$ cm $^2$	$l_{\text{sat}}/10^6$ cm	$v_g$ cms $^{-1}$	$\Gamma$ cm $^3$ s $^{-1}$	Mode
5	2.0589	64	-2.91E-13	32.3	1.91E+10	5.6E-03	OM
5	3.0889	69	-6.4E-14	129.4	2.28E+10	1.5E-03	XO
10	2.123	55	-6.72E-14	133.96	2.08E+10	1.4E-03	OM
20	2.285	41	-4.84E-15	1761.7	2.38E+10	1.1E-04	OM

**Table 6.**  $\nu_p/\nu_B = 1.8$ 

$T/10^6$ Kelvin	$\nu/\nu_B$	emission angle Degrees	$k_{\max}$ $\text{cm}^{-2}$	$l_{\text{sat}}/10^6$ cm	$v_g$ $\text{cms}^{-1}$	$\Gamma$ $\text{cm}^3\text{s}^{-1}$	Mode
5	2.04885	86.6	-2.65E-08	0.00019	6.45E+07	1.714	ZMN
5	2.0596	57	-1.5E-13	48.9	1.44E+10	2.2E-03	OM
5	3.0844	68	-5.4E-14	122.3	2.3E+10	1.1E-03	XO
10	2.1237	48	-3.97E-14	180.8	1.68E+10	6.7E-04	OM
10	3.1539	60	-1.94E-14	331.3	2.08E+10	4.03E-04	XO
20	2.2893	34	-2.24E-15	3045	2.18E+10	4.9E-05	OM

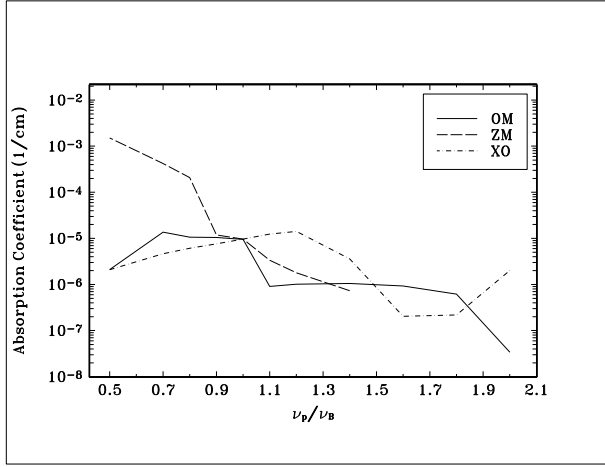


**Figure 1.** Largest in absolute value negative absorption coefficient as function of  $\nu_p/\nu_B$ , for the ZM, OM and XO mode. The calculation was performed with temperature of  $5 \cdot 10^6$  Kelvin,  $n_{\text{cold}}/n_{\text{hot}} = 10^4$ , power-law index of  $\delta = 3$ , low-energy cutoff of 10 keV, high energy cutoff of 1 MeV, loss cone parameters  $\cos(\alpha) = 0.81, \cos(\alpha - \Delta\alpha) = 0.83$ . The absorption coefficient given for any  $\nu_p/\nu_B$  is the largest in the entire frequency range  $\nu = \nu_B - 3\nu_B$ , and angle to magnetic field range  $\theta = 0 - 90$  degrees.

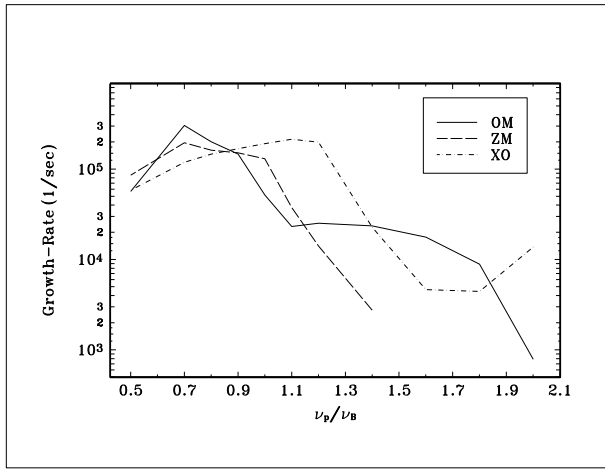


**Figure 2.** Largest growth rate as function of  $\nu_p/\nu_B$ , for the ZM, OM and XO mode. The calculation was performed with temperature of  $5 \cdot 10^6$  Kelvin,  $n_{\text{cold}}/n_{\text{hot}} = 10^4$ , power-law index of  $\delta = 3$ , low-energy cutoff of 10 keV, high energy cutoff of 1 MeV, loss cone parameters  $\cos(\alpha) = 0.81, \cos(\alpha - \Delta\alpha) = 0.83$ . The growth rate given for any  $\nu_p/\nu_B$  is the largest in the entire frequency range  $\nu = \nu_B - 3\nu_B$ , and angle to magnetic field range  $\theta = 0 - 90$  degrees. The largest growth rate does not necessarily occur at the same angle and frequency as the largest absolute value negative absorption.

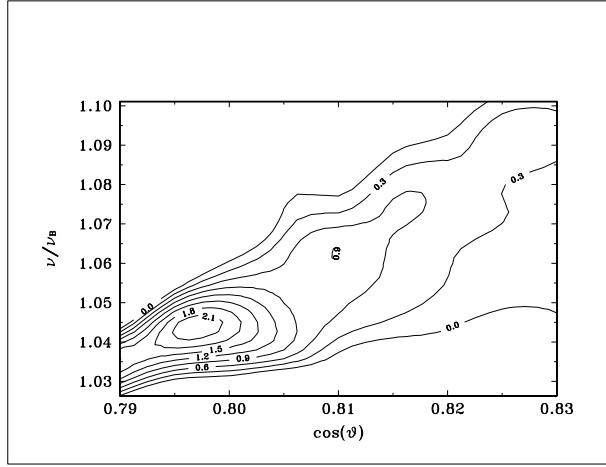


**Figure 3.** Contour map of the area surrounding the maximum negative absorption in the OM for  $\nu_p/\nu_B = 1$ , temperature  $T = 5 \cdot 10^6$  Kelvin, and  $n_{\text{cold}}/n_{\text{hot}} = 10^4$ . The x-axis of the figure denote  $\cos(\theta)$ , the y-axis denote the normalized frequency  $\nu/\nu_B$ , and the absorption coefficients are normalized to  $n_{\text{hot}} = 1$ , and multiplied by  $-10^{12}$

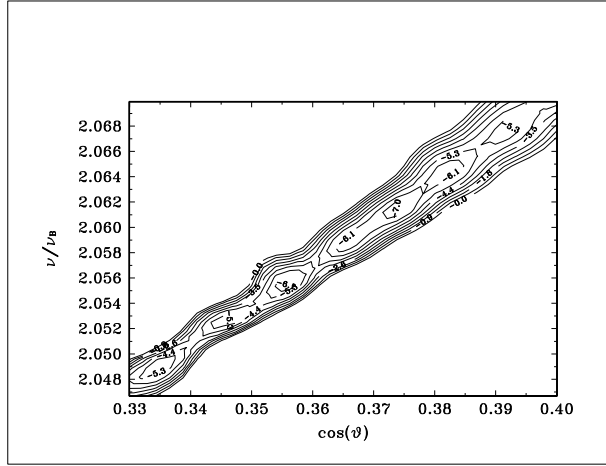


**Figure 4.** Contour map of the area surrounding the maximum negative absorption in the XO mode for  $\nu_p/\nu_B = 1$ , temperature  $T = 5 \cdot 10^6$  Kelvin, and  $n_{\text{cold}}/n_{\text{hot}} = 10^4$ . The x-axis of the figure denote  $\cos(\theta)$ , the y-axis denote the normalized frequency  $\nu/\nu_B$ , and the absorption coefficients are normalized to  $n_{\text{hot}} = 1$ , and multiplied by  $-10^{12}$

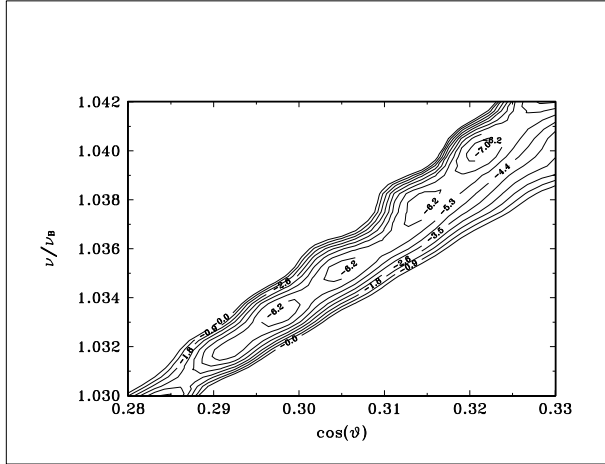


**Figure 5.** Contour map of the area surrounding the maximum negative absorption in the ZM for  $\nu_p/\nu_B = 1$ , temperature  $T = 5 \cdot 10^6$  Kelvin, and  $n_{\text{cold}}/n_{\text{hot}} = 10^4$ . The x-axis of the figure denote  $\cos(\theta)$ , the y-axis denote the normalized frequency  $\nu/\nu_B$ , and the absorption coefficients are normalized to  $n_{\text{hot}} = 1$ , and multiplied by  $-10^{12}$